Scientific Reports

https://doi.org/10.1038/s41598-026-50669-x

Article in Press

Exact traveling-wave solutions and dynamical behavior of nonlinear low-pass electrical models in the fractional framework

Received: 26 January 2026

Accepted: 22 April 2026

Published online: 02 May 2026

Cite this article as: Alsheekhhussain Z., Shah R., Sanaee H. *et al.* Exact traveling-wave solutions and dynamical behavior of nonlinear low-pass electrical models in the fractional framework. *Sci Rep* (2026). https://doi.org/10.1038/s41598-026-50669-x

Zainab Alsheekhhussain, Rasool Shah, Hashmatullah Sanaee, Saleh Alshammari, Mohammad Alshammari & M. Mossa Al-sawalha

Exact Traveling-Wave Solutions and Dynamical Behavior of Nonlinear Low-Pass Electrical Models in the Fractional Framework

Zainab Alsheekhhussain[1], Rasool Shah[2], Hashmatullah Sanaee[3,*], Saleh Alshammari[1], Mohammad Alshammari[1], M. Mossa Al-sawalha[1],

[1] Department of Mathematics, College of Science, University of Hail, Hail 2440, Saudi Arabia

Za.hussain@uoh.edu.sa, saleh.alshammari@uoh.edu.sa, dar.alshammari@uoh.edu.sa, m.alswalha@uoh.edu.sa

[2] Department of Mathematics, Abdul Wali Khan University Mardan Pakistan; rasoolshahawkum@gmail.com

[2] Department of Science, Kabul University, Kabul, Afghanistan; hashmatullah.sanaee@ku.edu.af

*Corresponding author: hashmatullah.sanaee@ku.edu.af (Hashmatullah Sanaee)

April 22, 2026

Abstract

The paper is an analytical study of a low-pass electrical model of nonlinear type in a fractional perspective, in which the classical derivative is generalized to the Katugampola fractional operator. Precise traveling-wave solutions are built based on an extended Riccati-Bernoulli sub-ODE scheme together with a Bäcklund transformation. The families of obtained solutions contain bright and dark kink type structures. These solutions have a dynamical behavior that is demonstrated with the help of detailed 3D and 2D visualizations. The 3D plots reveal how sensitive the integer-order parameter is to the waveform whereas the 2D plots show how sensitive the waveform is to the changes in the fractional order (α). To deeper examine the qualitative dynamics, a hamiltonian formulation is created and phase-portrait diagrams are plotted. These unveil the local and global organization of the nonlinear flow underlying. Besides, chaotic behavior is also studied by analyzing sensitivity to initial conditions by determining the largest Lyapunov exponent λ_{max}. The findings validate the occurrence of regular, quasi-periodic and chaotic regimes in the parameter space. The entire process of analytical calculations and visualization is implemented in MATLAB, which provides the numerical accuracy of calculations and high-resolution graphical confirmation of fractions solutions. The results illustrate the presence of significant enrichment of the dynamical behavior of the nonlinear electrical model by the fractional extension. It also offers a practical and efficient model to study intricate waves phenomena in the systems of the fractional-order.

Keywords:

Low pass electric line, solitary wave analysis, Katugampola fractional derivative (KFD), Bifurcation, Bäcklund transformation.

1 Introduction:

The study of nonlinear partial differential equations (NLPDEs) is the mathematical basis of the investigation of nonlinear physical processes, and is the mathematical basis of a large variety of nonlinear wave interactions. This is a natural occurrence in many technical, medical, and scientific applications of waves [1]. The inherent complexity and nonlinearity of these models has led to the growing use of computational methods in overcoming analytical difficulties related to NLPDEs [2]. These are large-scale methods of numerical modeling and analysis of nonlinear evolution equations (NLEEs) [3]. Besides numerical methods, diverse sophisticated tools of analysis have been established to build precise solutions of NLEEs [4–8]. The most common are Lie symmetry methods [9], the Darboux transformation [10], all of which provide systematic ways of constructing new solutions out of known ones. The other prominent methods are the Hirota bilinear method [11, 12] and the generalized exponential rational function (GERF) method [13], and a few other contemporary methods of analysis. Nonlinear PDEs may have a very diverse range of solution structures, kink and anti-kink solutions being particularly significant. These solutions are localized changes between different asymptotic states, which are commonly known to be stable, robust and physically relevant in nonlinear dynamical systems [14–16]. Kink-type structures have special significance to the dynamics of nonlinear wave propagation and interaction because they occur in both integrable and non-integrable models. A number of works have examined kink solutions, their fractional extensions, and how they interact with other complete solution families, which leads to a highly rich and complicated dynamical structure being realized in the context of systems of nonlinear equations of fractional order [17].

The electrical transmission line equation is a fundamental concept in communication systems and electronic engineering because it is extensively used in mobile communication networks, computer interconnection systems, switching circuits, high-speed data buses, radio transmitter-receiver links, antenna coupling, and cable-TV signal distribution networks [18]. In the classical context the low-pass electrical transmission line model (LPETLM) can be characterized using the voltage $\mathcal{P}(x,t)$ of the model which is a function of the space coordinate (x) and time (t) and (β), (γ) and (μ) are the real constants, as follows [19, 20]:

$$\frac{\partial^2 \mathcal{P}(x,t)}{\partial t^2} - \beta \frac{\partial^2 \mathcal{P}^2(x,t)}{\partial t^2} + \gamma \frac{\partial^2 \mathcal{P}^3(x,t)}{\partial t^2} - \mu^2 \frac{\partial^2 \mathcal{P}(x,t)}{\partial x^2} + \frac{\mu^4}{12} \frac{\partial^4 \mathcal{P}(x,t)}{\partial x^4} = 0. \tag{1}$$

Several analytical schemes have been offered over the years to solve the equation (1). These are modified simple equation technique [21], the new mapping technique, the extended auxiliary equation technique, and the extended Kudryashkov technique [22]. Alternatively, modified Kudryashov method, sine-Gordon expansion, and its higher extensions have been considered to find solutions [23]. Simultaneously with such advances, fractional and fractal calculus have now become important in the modeling

of complex systems in biomedical dynamics [24], circuit theory [25], and electrical engineering [26]. As an example, [27] used the Atangana-Baleanu derivative to explore the equation (1). By cubic and septic B-spline schemes, and conformal versions of the LPETLM were examined by the extended direct algebraic method in [28]. Furthermore, a fractional LPETLM was presented in [29] using the modified Riemann-Liouville operator and solved using the Exp-function approach to a number of different soliton structures. More recently, it has been shown that neural network approaches to neural network-based methods are effective in the analysis and solution of partial differential equations and that they offer flexible and efficient computational methods of complex nonlinear systems [30–32]. Such practices in combination with analytical and numerical approaches could provide supplementary information and a deeper comprehension of solution strategies. The relevance of the classical methods of fractional-order analysis with the contemporary machine learning frameworks has been increasing, as highlighted by these studies [33–37]. The nonlinear low-pass electrical model developed based on the nonlinearity inherent in the elements of the circuits of this paper, leading to a governing equation that embodies the nonlinearity of the circuit in both voltage and current. We replace the governing equation with the Katugampola fractional derivative to generalize the model, and to be able to consider the effects of memory of real electrical components.

Driven by these developments, and acknowledging the constraints of integer-order and earlier introduced operators of the fractional calculus, the current work constructs a fractional LPETLM based on the Katugampola fractional derivative, an effective operator in systems with nonlocal memory, porous-media dynamics and complex scaling modes. The model would also become the classical LPETLM, when ($\alpha \to 1$), where (α) is the Katugampola fractional order parameter.

$$D_t^{2\alpha}\,\mathcal{P}(x,t) - \beta\, D_t^{2\alpha}\Big(\mathcal{P}^2(x,t)\Big) + \gamma\, D_t^{2\alpha}\Big(\mathcal{P}^3(x,t)\Big) - \mu^2\, D_x^{2\alpha}\,\mathcal{P}(x,t) + \frac{\mu^4}{12}\, D_x^{4\alpha}\,\mathcal{P}(x,t) = 0. \tag{2}$$

In equation (2), $\mathcal{D}^{\alpha}$ represent the fractional derivative of order α, where $0 < \alpha \leq 1$. Katugampola fractional derivative is selected in this work due to its generalized form that integrates the properties of classical fractional derivatives like the Riemann-Liuvelve and the Hadamard derivatives. In contrast to standard definitions, the Katugampola operator uses a scaling parameter to offer extra flexibility in the representation of nonlocal effects and heterogeneous memory characteristics of nonlinear electrical transmission systems. This causes it to be especially appropriate in the modeling of wave propagation in media where power-law behavior and the presence of logarithmic scaling can both occur. The Katugampola derivative provides a more flexible model of describing complex dynamical characteristics as compared to other popular fractional derivatives, like the Caputo and Atangana-Baleanu operators, without losing analytical tractability. In order to obtain analytical solutions of this fractional model, we use a generalized Riccati-Bernoulli sub-ODE method together with a Bäcklund transformation that gives us closed form bright and dark kink solutions [38–40]. These solutions are then studied with detailed Hamiltonian dynamics, phase-portrait construction, chaotic sensitivity diagnostics, and the computation of the maximum Lyapunov exponent. The rest of the present paper proceeds as follows:

Section 2 outlines the Riccati-Bernoulli sub-ODE model with corresponding Bäcklund transformation, Section 3 is the presentation of the analytical kink-type solutions, followed by graphical and dynamical analysis in Section 4 alongside the discussion of the Hamiltonian and chaotic behavior, and Section 5

concludes the paper.

In the current study, the operator $\mathcal{D}^{\alpha}$ represents the Katugampola fractional derivative (KFD) of order $0 < \alpha \leq 1$, the basis fractional operator of our fractional extension of the low-pass electrical transmission line model. The Katugampola operator, unlike the classical integer-order differentiation, has intrinsic memory, nonlocality, and hereditary effects, allowing a more realistic description of complex electrical transmission processes in heterogeneous or anomalous media. In the context of our work, the Katugampola derivative is used in the voltage dependent field variable $\mathcal{P}(x,t)$, which is used to determine the occurrence of the bright and dark kink-type wave structures. In reference to [41], the Katugampola fractional derivative of a sufficiently smooth $H(x,t)$ formal definition is as follows:

$$\mathcal{D}_t^{\alpha}\mathcal{H}(t) = \lim_{\varepsilon \to 0} \frac{\mathcal{H}\left(t\, e^{\varepsilon\, t^{-\alpha}}\right) - \mathcal{H}(t)}{\varepsilon}, \quad t > 0,\ 0 < \alpha \leq 1. \tag{3}$$

The KFD satisfies several important properties that are useful in fractional modeling:

$$\begin{cases} \mathcal{D}_t^{\alpha}\left(a\mathcal{H}(t) + bG(t)\right) = a\,\mathcal{D}_t^{\alpha}\mathcal{H}(t) + b\,\mathcal{D}_t^{\alpha}G(t), \\ \mathcal{D}_t^{\alpha}(t^k) = k\,t^{k-\alpha}, \quad k > 0, \\ \mathcal{D}_t^{\alpha}\left(\mathcal{H}(t)G(t)\right) = \mathcal{H}(t)\,\mathcal{D}_t^{\alpha}G(t) + G(t)\,\mathcal{D}_t^{\alpha}\mathcal{H}(t), \\ \mathcal{D}_t^{\alpha}\left(\mathcal{H}(G(t))\right) = \mathcal{H}'(G(t))\,\mathcal{D}_t^{\alpha}G(t), \\ \lim\limits_{\alpha \to 1} \mathcal{D}_t^{\alpha}\mathcal{H}(t) = \dfrac{d\mathcal{H}(t)}{dt}. \end{cases} \tag{4}$$

2 Methodology:

The current work constructs a stringent fractional analytical structure on the study of the nonlinear behaviours of the low-pass electrical transmission line model (LPETLM) developed in the Katugampola space-time fractional calculus. There are four basic elements of our methodology:

(i) Fractional extension of the LPETLM using the Katugampola derivative to measure memory-based electrical transport effects.

(ii) Travelling-wave reduction and a Bäcklund-assisted transformation, which allows the governing PDE to be transformed into a nonlinear fractional ODE solvable term.

(iii) Generalized Riccati-Bernoulli sub-ODE scheme to find explicit bright and dark kink solutions and categorize the resulting families of waveforms in integer and fractional order.

(iv) Advanced dynamical analysis, such as checking of the Hamiltonian structure, characterization of phase portraits, sensitivity analysis, detection of chaotic regimes and calculation of the largest Lyapunov exponent.

Step. 1:

Nonlocal, memory-driven, and hereditary effects naturally occurring in complicated electromagnetic and electrical transport media are reformulated in the low-pass electrical transmission line model (LPETLM) in the framework of the Katugampola space-time fractional derivative (α). The Katugampola

derivative is especially adapted to the long-range temporal correlations and spatially nonlocal interactions and a more realistic description of anomalous propagation in fractal or porous conductors. The generalized fractional LPETLM may be abstractly represented as

$$\mathcal{Z}_1\left(\mathcal{P}, \mathcal{D}_t^{\alpha}\mathcal{P}, \mathcal{D}_x^{\alpha}\mathcal{P}, \mathcal{D}_x^{2\alpha}\mathcal{P}, \mathcal{P}\mathcal{D}_x^{\alpha}\mathcal{P}, \ldots\right) = 0, \quad 0 < \alpha \leq 1, \tag{5}$$

$\mathcal{P}$, represents the potential field of transmission line. The strength of memory, nonlocal dispersion, and long-distance coupling is controlled by the fractional parameter (α), enabling the model to capture delay-type responses and anomalous wave transport that are not accessible in the classical integer-order LPETLM.

Step. 2:

The fractional PDE is simplified to an ODE by a Katugampola type travelling wave similarity variable,

$$\psi = \sqrt{k}\left(\frac{x^{\alpha}}{\alpha} - \frac{\omega\, t^{\alpha}}{\alpha}\right), \tag{6}$$

Using the properties of the Katugampola fractional derivative, the temporal and spatial fractional derivatives are transformed into integer order derivatives with respect to the wave variable (ψ) as follows:

$$D_t^{2\alpha} \longrightarrow \omega^2 \frac{d^2}{d\psi^2}, \qquad D_x^{2\alpha} \longrightarrow k\frac{d^2}{d\psi^2}. \tag{7}$$

By replacing the transformation of (6) with the equation (2) the fractional partial differential equation is simplified to a second-order nonlinear ordinary differential equation. It should be mentioned that the fractional-order parameter (α) is also implicitly present in the transformed variable (ψ), hence affecting the reduced dynamical system. In order to get nonlinear excitations in closed-form, we use the nonlinear flexible ansatz, which represents the variability of amplitude and multi-scale deflections in the fractional media:

$$F(\psi) = \sum_{i=-n}^{n} m_i\, \chi(\psi)^i, \tag{8}$$

where, $\chi(\zeta)$ is defined via the Bäcklund transformation:

$$\chi(\zeta) = \frac{-\mathcal{S}c_2 + c_1\mathcal{W}(\psi)}{c_1 + c_2\mathcal{W}(\psi)}, \tag{9}$$

and ($\mathcal{W}$) satisfies the generalized Riccati-Bernoulli equation,

$$\frac{d\mathcal{W}}{d\psi} = \mathcal{S} + \mathcal{W}(\psi)^2. \tag{10}$$

Step. 3:

The reduced Katugampola space time fractional framework puts the nonlinear wave dynamics entirely dependent on the discriminant parameter $\mathcal{S}$, which classifies the solution space produced via the Riccati Bernoulli Bäcklund construction. It is a parameter that determines the qualitative rank of the fractional nonlinear waves that are defined by the governing ODE:

- $\mathcal{S} > 0 \longrightarrow$ trigonometric family: periodic oscillatory structures associated with modulation insta-

bility and periodically breathing optical modes.

- $\mathcal{S} < 0 \longrightarrow$ hyperbolic family: localized solitonic or breather type structures, including dark, bright, kink and singular modes.
- $\mathcal{S} = 0 \longrightarrow$ rational family: slowly decaying waveforms, algebraic breathers, and rogue-like transients.

These families come about because of generalized trigonometric and hyperbolic functions, $(\sin_{\kappa\nu}, \cos_{\kappa\nu}, \sinh_{\kappa\nu}, \tanh_{\kappa\nu}, \ldots)$, which occur naturally as a result of the combined action of fractional dispersion and nonlinear interactions. The resultant waves have asymmetry, amplitude modulation, and kink soliton which is customized by both the discriminant and the fractional-order parameter (α).

Step. 4:

The behavior of the physical objects that are inherent in the analytical solutions of the Katugampola space-time fractional model is revealed by using a cohesive visualization-dynamical-systems framework. The classical limit is associated with the 3D surface plots, ($\alpha = 1$) which depicts the complete morphology of the bright and dark solutions of the kink type, their amplitude deformation, transition layers, and propagation features. The complementary 2D profiles demonstrate the continuous restructuring of the wave structure by the fractional-order parameter ($\alpha < 1$), which facilitates the change among classical, fractional dynamics by changing steepness, width, and asymmetry. A dynamical-systems analysis is done in order to learn more about the nonlinear evolution. Phase portraits and hamiltonian energy landscapes are measures of the qualitative dynamics of the simple system, and Lyapunov exponents and chaotic sensitivity diagnostics are measures of instability regimes and the transition to complex excitations. Spatial energy-density distribution is also examined providing a hint on the localization of waves, trapping, and transport of waves in the fractional medium.

3 Application of the proposed method:

Now we concentrate upon solitary wave solutions of the system of equation (2). Using the travelling wave transformation (6) and replacing it on the fractional model, the governing PDE simplifies to the following ordinary differential equation.

$$\frac{k\mu^4}{12}\frac{d^4F}{d\psi^4} + \left(\mu^2 - \omega^2\right)\frac{d^2F}{d\psi^2} + \beta\omega^2\frac{d^2(F)^2}{d\psi^2} - \gamma\omega^2\frac{d^2(F)^3}{d\psi^2} = 0. \tag{11}$$

Integrating equation (11) twice and setting the integral constant as zero, yields:

$$\frac{k\mu^4}{12}\frac{d^2F}{d\psi^2} + \left(\mu^2 - \omega^2\right)F + \beta\omega^2F^2 - \gamma\omega^2F^3 = 0. \tag{12}$$

Using the Principle of balancing between the highest derivative term $\frac{d^2F}{d\psi^2}$ and the nonlinear one F^3 of equation (12), we obtain $n = 1$, substituting in equation (8), we get,

$$F(\psi) = m_{-1}\Big(\chi(\psi)\Big)^{-1} + m_0 + m_1\Big(\chi(\psi)\Big)^{1}. \tag{13}$$

Substituting equation (13) into equation (12) with equation (8) and equation (9) and setting the coefficients equal to zero we get an algebraic system. By resolving this algebraic system, the unknown parameters can be determined and this can be used to explicitly build the analytical solutions.

$$m_1 = \frac{1}{18}\frac{\beta^2}{\gamma^2 m_{-1}}, m_{-1} = m_{-1}, m_0 = \frac{1}{3}\frac{\beta}{\gamma}, k = \frac{1}{6}\frac{\beta^4}{\gamma^2 {m_{-1}}^2 \mu^2 (-2\beta^2 + 9\gamma)}, \omega = 3\sqrt{-\frac{\gamma}{2\beta^2 - 9\gamma}}\mu, \mathcal{S} = 18\frac{\gamma^2 {m_{-1}}^2}{\beta^2}. \tag{14}$$

For ($\mathcal{S} < 0$), the KFD framework yields hyperbolic-type fractional wave solutions.

$$\mathcal{P}_1(x,t) = \frac{m_{-1}\left(c_1 - c_2\sqrt{-\mathcal{S}}\tanh\left(\sqrt{-\mathcal{S}}\psi\right)\right)}{-\mathcal{S}c_2 - c_1\sqrt{-\mathcal{S}}\tanh\left(\sqrt{-\mathcal{S}}\psi\right)} + \frac{1}{3}\frac{\beta}{\gamma} + \frac{1}{18}\frac{\beta^2\left(-\mathcal{S}c_2 - c_1\sqrt{-\mathcal{S}}\tanh\left(\sqrt{-\mathcal{S}}\psi\right)\right)}{\gamma^2 m_{-1}\left(c_1 - c_2\sqrt{-\mathcal{S}}\tanh\left(\sqrt{-\mathcal{S}}\psi\right)\right)}, \tag{15}$$

$$\mathcal{P}_2(x,t) = \frac{m_{-1}\left(c_1 - c_2\sqrt{-\mathcal{S}}\coth\left(\sqrt{-\mathcal{S}}\psi\right)\right)}{-\mathcal{S}c_2 - c_1\sqrt{-\mathcal{S}}\coth\left(\sqrt{-\mathcal{S}}\psi\right)} + \frac{1}{3}\frac{\beta}{\gamma} + \frac{1}{18}\frac{\beta^2\left(-\mathcal{S}c_2 - c_1\sqrt{-\mathcal{S}}\coth\left(\sqrt{-\mathcal{S}}\psi\right)\right)}{\gamma^2 m_{-1}\left(c_1 - c_2\sqrt{-\mathcal{S}}\coth\left(\sqrt{-\mathcal{S}}\psi\right)\right)}, \tag{16}$$

$$\mathcal{P}_3(x,t) = \frac{m_{-1}\left(c_1 + c_2\left(-\sqrt{-\mathcal{S}}\tanh\left(2\sqrt{-\mathcal{S}}\psi\right) \pm \left(i\sqrt{-\mathcal{S}}sech\left(2\sqrt{-\mathcal{S}}\psi\right)\right)\right)\right)}{-\mathcal{S}c_2 + c_1\left(-\sqrt{-\mathcal{S}}\tanh\left(2\sqrt{-\mathcal{S}}\psi\right) \pm \left(i\sqrt{-\mathcal{S}}sech\left(2\sqrt{-\mathcal{S}}\psi\right)\right)\right)} + \frac{1}{3}\frac{\beta}{\gamma} + \frac{1}{18}\frac{\beta^2\left(-\mathcal{S}c_2 + c_1\left(-\sqrt{-\mathcal{S}}\tanh\left(2\sqrt{-\mathcal{S}}\psi\right) \pm \left(i\sqrt{-\mathcal{S}}sech\left(2\sqrt{-\mathcal{S}}\psi\right)\right)\right)\right)}{\gamma^2 m_{-1}\left(c_1 + c_2\left(-\sqrt{-\mathcal{S}}\tanh\left(2\sqrt{-\mathcal{S}}\psi\right) \pm \left(i\sqrt{-\mathcal{S}}sech\left(2\sqrt{-\mathcal{S}}\psi\right)\right)\right)\right)}, \tag{17}$$

$$\mathcal{P}_4(x,t) = \frac{m_{-1}\left(c_1 + c_2\left(-\sqrt{-\mathcal{S}}\coth\left(2\sqrt{-\mathcal{S}}\psi\right) \pm \left(\sqrt{-\mathcal{S}}csch\left(2\sqrt{-\mathcal{S}}\psi\right)\right)\right)\right)}{-\mathcal{S}c_2 + c_1\left(-\sqrt{-\mathcal{S}}\coth\left(2\sqrt{-\mathcal{S}}\psi\right) \pm \left(\sqrt{-\mathcal{S}}csch\left(2\sqrt{-\mathcal{S}}\psi\right)\right)\right)} + \frac{1}{3}\frac{\beta}{\gamma} + \frac{1}{18}\frac{\beta^2\left(-\mathcal{S}c_2 + c_1\left(-\sqrt{-\mathcal{S}}\coth\left(2\sqrt{-\mathcal{S}}\psi\right) \pm \left(\sqrt{-\mathcal{S}}csch\left(2\sqrt{-\mathcal{S}}\psi\right)\right)\right)\right)}{\gamma^2 m_{-1}\left(c_1 + c_2\left(-\sqrt{-\mathcal{S}}\coth\left(2\sqrt{-\mathcal{S}}\psi\right) \pm \left(\sqrt{-\mathcal{S}}csch\left(2\sqrt{-\mathcal{S}}\psi\right)\right)\right)\right)}, \tag{18}$$

$$\mathcal{P}_5(x,t) = \frac{m_{-1}\left(c_1 + c_2\left(-\frac{1}{2}\sqrt{-\mathcal{S}}\tanh\left(\frac{1}{2}\sqrt{-\mathcal{S}}\psi\right) - \frac{1}{2}\sqrt{-\mathcal{S}}\coth\left(\frac{1}{2}\sqrt{-\mathcal{S}}\psi\right)\right)\right)}{-\mathcal{S}c_2 + c_1\left(-\frac{1}{2}\sqrt{-\mathcal{S}}\tanh\left(\frac{1}{2}\sqrt{-\mathcal{S}}\psi\right) - \frac{1}{2}\sqrt{-\mathcal{S}}\coth\left(\frac{1}{2}\sqrt{-\mathcal{S}}\psi\right)\right)} + \frac{1}{3}\frac{\beta}{\gamma} + \frac{1}{18}\frac{\beta^2\left(-\mathcal{S}c_2 + c_1\left(-\frac{1}{2}\sqrt{-\mathcal{S}}\tanh\left(\frac{1}{2}\sqrt{-\mathcal{S}}\psi\right) - \frac{1}{2}\sqrt{-\mathcal{S}}\coth\left(\frac{1}{2}\sqrt{-\mathcal{S}}\psi\right)\right)\right)}{\gamma^2 m_{-1}\left(c_1 + c_2\left(-\frac{1}{2}\sqrt{-\mathcal{S}}\tanh\left(\frac{1}{2}\sqrt{-\mathcal{S}}\psi\right) - \frac{1}{2}\sqrt{-\mathcal{S}}\coth\left(\frac{1}{2}\sqrt{-\mathcal{S}}\psi\right)\right)\right)}, \tag{19}$$

$$\mathcal{P}_6(x,t) = \frac{m_{-1}\left(c_1 + \frac{c_2\left(\sqrt{-(\tau^2+\varsigma^2)\mathcal{S}} - \tau\sqrt{-\mathcal{S}}\cosh\left(2\sqrt{-\mathcal{S}}\psi\right)\right)}{\tau\sinh\left(2\sqrt{-\mathcal{S}}\psi\right)+\varsigma}\right)}{\left(-\mathcal{S}c_2 + \frac{c_1\left(\sqrt{-(\tau^2+\varsigma^2)\mathcal{S}} - \tau\sqrt{-\mathcal{S}}\cosh\left(2\sqrt{-\mathcal{S}}\psi\right)\right)}{\tau\sinh\left(2\sqrt{-\mathcal{S}}\psi\right)+\varsigma}\right)} + \frac{1}{3}\frac{\beta}{\gamma} + \frac{1}{18}\frac{\beta^2\left(-\mathcal{S}c_2 + \frac{c_1\left(\sqrt{-(\tau^2+\varsigma^2)\mathcal{S}} - \tau\sqrt{-\mathcal{S}}\cosh\left(2\sqrt{-\mathcal{S}}\psi\right)\right)}{\tau\sinh\left(2\sqrt{-\mathcal{S}}\psi\right)+\varsigma}\right)}{\gamma^2 m_{-1}\left(c_1 + \frac{c_2\left(\sqrt{-(\tau^2+\varsigma^2)\mathcal{S}} - \tau\sqrt{-\mathcal{S}}\cosh\left(2\sqrt{-\mathcal{S}}\psi\right)\right)}{\tau\sinh\left(2\sqrt{-\mathcal{S}}\psi\right)+\varsigma}\right)}, \tag{20}$$

$$\mathcal{P}_7(x,t) = \frac{m_{-1}\left(c_1 + \frac{c_2\left(\sqrt{-(\varsigma^2-\tau^2)\mathcal{S}} - \tau\sqrt{-\mathcal{S}}\sinh\left(2\sqrt{-\mathcal{S}}\psi\right)\right)}{\tau\cosh\left(2\sqrt{-\mathcal{S}}\psi\right)+\varsigma}\right)}{\left(-\mathcal{S}c_2 + \frac{c_1\left(\sqrt{-(\varsigma^2-\tau^2)\mathcal{S}} - \tau\sqrt{-\mathcal{S}}\sinh\left(2\sqrt{-\mathcal{S}}\psi\right)\right)}{\tau\cosh\left(2\sqrt{-\mathcal{S}}\psi\right)+\varsigma}\right)} + \frac{1}{3}\frac{\beta}{\gamma} + \frac{1}{18}\frac{\beta^2\left(-\mathcal{S}c_2 + \frac{c_1\left(\sqrt{-(\varsigma^2-\tau^2)\mathcal{S}} - \tau\sqrt{-\mathcal{S}}\sinh\left(2\sqrt{-\mathcal{S}}\psi\right)\right)}{\tau\cosh\left(2\sqrt{-\mathcal{S}}\psi\right)+\varsigma}\right)}{\gamma^2 m_{-1}\left(c_1 + \frac{c_2\left(\sqrt{-(\varsigma^2-\tau^2)\mathcal{S}} - \tau\sqrt{-\mathcal{S}}\sinh\left(2\sqrt{-\mathcal{S}}\psi\right)\right)}{\tau\cosh\left(2\sqrt{-\mathcal{S}}\psi\right)+\varsigma}\right)}. \tag{21}$$

For ($\mathcal{S} > 0$), the KFD framework yields trigonometric-type fractional wave solutions.

$$\mathcal{P}_8(x,t) = \frac{m_{-1}\left(c_1 + c_2\sqrt{\mathcal{S}}\tan\left(\sqrt{\mathcal{S}}\psi\right)\right)}{-\mathcal{S}c_2 + c_1\sqrt{\mathcal{S}}\tan\left(\sqrt{\mathcal{S}}\psi\right)} + \frac{1}{3}\frac{\beta}{\gamma} + \frac{1}{18}\frac{\beta^2\left(-\mathcal{S}c_2 + c_1\sqrt{\mathcal{S}}\tan\left(\sqrt{\mathcal{S}}\psi\right)\right)}{\gamma^2 m_{-1}\left(c_1 + c_2\sqrt{\mathcal{S}}\tan\left(\sqrt{\mathcal{S}}\psi\right)\right)}, \tag{22}$$

$$\mathcal{P}_9(x,t) = \frac{m_{-1}\left(c_1 - c_2\sqrt{\mathcal{S}}\cot\left(\sqrt{\mathcal{S}}\psi\right)\right)}{-\mathcal{S}c_2 - c_1\sqrt{\mathcal{S}}\cot\left(\sqrt{\mathcal{S}}\psi\right)} + \frac{1}{3}\frac{\beta}{\gamma} + \frac{1}{18}\frac{\beta^2\left(-\mathcal{S}c_2 - c_1\sqrt{\mathcal{S}}\cot\left(\sqrt{\mathcal{S}}\psi\right)\right)}{\gamma^2 m_{-1}\left(c_1 - c_2\sqrt{\mathcal{S}}\cot\left(\sqrt{\mathcal{S}}\psi\right)\right)}, \tag{23}$$

$$\mathcal{P}_{10}(x,t) = \frac{m_{-1}\left(c_1 + c_2\left(-\sqrt{\mathcal{S}}\tan\left(2\sqrt{\mathcal{S}}\psi\right) \pm \left(\sqrt{\mathcal{S}}\sec\left(2\sqrt{\mathcal{S}}\psi\right)\right)\right)\right)}{-\mathcal{S}c_2 + c_1\left(-\sqrt{\mathcal{S}}\tan\left(2\sqrt{\mathcal{S}}\psi\right) \pm \left(\sqrt{\mathcal{S}}\sec\left(2\sqrt{\mathcal{S}}\psi\right)\right)\right)} + \frac{1}{3}\frac{\beta}{\gamma} + \frac{1}{18}\frac{\beta^2\left(-\mathcal{S}c_2 + c_1\left(-\sqrt{\mathcal{S}}\tan\left(2\sqrt{\mathcal{S}}\psi\right) \pm \left(\sqrt{\mathcal{S}}\sec\left(2\sqrt{\mathcal{S}}\psi\right)\right)\right)\right)}{\gamma^2 m_{-1}\left(c_1 + c_2\left(-\sqrt{\mathcal{S}}\tan\left(2\sqrt{\mathcal{S}}\psi\right) \pm \left(\sqrt{\mathcal{S}}\sec\left(2\sqrt{\mathcal{S}}\psi\right)\right)\right)\right)}, \tag{24}$$

$$\mathcal{P}_{11}(x,t) = \frac{m_{-1}\left(c_1 + c_2\left(-\sqrt{\mathcal{S}}\cot\left(2\sqrt{\mathcal{S}}\psi\right) \pm \left(\sqrt{\mathcal{S}}\csc\left(2\sqrt{\mathcal{S}}\psi\right)\right)\right)\right)}{-\mathcal{S}c_2 + c_1\left(-\sqrt{\mathcal{S}}\cot\left(2\sqrt{\mathcal{S}}\psi\right) \pm \left(\sqrt{\mathcal{S}}\csc\left(2\sqrt{\mathcal{S}}\psi\right)\right)\right)} + \frac{1}{3}\frac{\beta}{\gamma} + \frac{1}{18}\frac{\beta^2\left(-\mathcal{S}c_2 + c_1\left(-\sqrt{\mathcal{S}}\cot\left(2\sqrt{\mathcal{S}}\psi\right) \pm \left(\sqrt{\mathcal{S}}\csc\left(2\sqrt{\mathcal{S}}\psi\right)\right)\right)\right)}{\gamma^2 m_{-1}\left(c_1 + c_2\left(-\sqrt{\mathcal{S}}\cot\left(2\sqrt{\mathcal{S}}\psi\right) \pm \left(\sqrt{\mathcal{S}}\csc\left(2\sqrt{\mathcal{S}}\psi\right)\right)\right)\right)}, \tag{25}$$

$$\mathcal{P}_{12}(x,t) = \frac{m_{-1}\left(c_1 + c_2\left(\frac{1}{2}\sqrt{\mathcal{S}}\tan\left(\frac{1}{2}\sqrt{\mathcal{S}}\psi\right) - \frac{1}{2}\sqrt{\mathcal{S}}\cot\left(\frac{1}{2}\sqrt{\mathcal{S}}\psi\right)\right)\right)}{-\mathcal{S}c_2 + c_1\left(\frac{1}{2}\sqrt{\mathcal{S}}\tan\left(\frac{1}{2}\sqrt{\mathcal{S}}\psi\right) - \frac{1}{2}\sqrt{\mathcal{S}}\cot\left(\frac{1}{2}\sqrt{\mathcal{S}}\psi\right)\right)} + \frac{1}{3}\frac{\beta}{\gamma} + \frac{1}{18}\frac{\beta^2\left(-\mathcal{S}c_2 + c_1\left(\frac{1}{2}\sqrt{\mathcal{S}}\tan\left(\frac{1}{2}\sqrt{\mathcal{S}}\psi\right) - \frac{1}{2}\sqrt{\mathcal{S}}\cot\left(1/2\sqrt{\mathcal{S}}\psi\right)\right)\right)}{\gamma^2 m_{-1}\left(c_1 + c_2\left(\frac{1}{2}\sqrt{\mathcal{S}}\tan\left(\frac{1}{2}\sqrt{\mathcal{S}}\psi\right) - \frac{1}{2}\sqrt{\mathcal{S}}\cot\left(\frac{1}{2}\sqrt{\mathcal{S}}\psi\right)\right)\right)}, \tag{26}$$

$$\mathcal{P}_{13}(x,t) = \frac{m_{-1}\left(c_1 + \frac{c_2\left(\pm\left(\sqrt{(-\varsigma^2+\tau^2)\mathcal{S}}\right) - \tau\sqrt{\mathcal{S}}\cos\left(2\sqrt{\mathcal{S}}\psi\right)\right)}{\tau\sin\left(2\sqrt{\mathcal{S}}\psi\right)+\varsigma}\right)}{\left(-\mathcal{S}c_2 + \frac{c_1\left(\pm\left(\sqrt{(-\varsigma^2+\tau^2)\mathcal{S}}\right) - \tau\sqrt{\mathcal{S}}\cos\left(2\sqrt{\mathcal{S}}\psi\right)\right)}{\tau\sin\left(2\sqrt{\mathcal{S}}\psi\right)+\varsigma}\right)} + \frac{1}{3}\frac{\beta}{\gamma} + \frac{1}{18}\frac{\beta^2\left(-\mathcal{S}c_2 + \frac{c_1\left(\pm\left(\sqrt{(-\varsigma^2+\tau^2)\mathcal{S}}\right) - \tau\sqrt{\mathcal{S}}\cos\left(2\sqrt{\mathcal{S}}\psi\right)\right)}{\tau\sin\left(2\sqrt{\mathcal{S}}\psi\right)+\varsigma}\right)}{\gamma^2 m_{-1}\left(c_1 + \frac{c_2\left(\pm\left(\sqrt{(-\varsigma^2+\tau^2)\mathcal{S}}\right) - \tau\sqrt{\mathcal{S}}\cos\left(2\sqrt{\mathcal{S}}\psi\right)\right)}{\tau\sin\left(2\sqrt{\mathcal{S}}\psi\right)+\varsigma}\right)}, \tag{27}$$

$$\mathcal{P}_{14}(x,t) = \frac{m_{-1}\left(c_1 + \frac{c_2\left(\pm\left(\sqrt{(-\varsigma^2+\tau^2)\mathcal{S}}\right) - \tau\sqrt{\mathcal{S}}\sin\left(2\sqrt{\mathcal{S}}\psi\right)\right)}{\tau\cos\left(2\sqrt{\mathcal{S}}\psi\right)+\varsigma}\right)}{\left(-\mathcal{S}c_2 + \frac{c_1\left(\pm\left(\sqrt{(-\varsigma^2+\tau^2)\mathcal{S}}\right) - \tau\sqrt{\mathcal{S}}\sin\left(2\sqrt{\mathcal{S}}\psi\right)\right)}{\tau\cos\left(2\sqrt{\mathcal{S}}\psi\right)+\varsigma}\right)} + \frac{1}{3}\frac{\beta}{\gamma} + \frac{1}{18}\frac{\beta^2\left(-\mathcal{S}c_2 + \frac{c_1\left(\pm\left(\sqrt{(-\varsigma^2+\tau^2)\mathcal{S}}\right) - \tau\sqrt{\mathcal{S}}\sin\left(2\sqrt{\mathcal{S}}\psi\right)\right)}{\tau\cos\left(2\sqrt{\mathcal{S}}\psi\right)+\varsigma}\right)}{\gamma^2 m_{-1}\left(c_1 + \frac{c_2\left(\pm\left(\sqrt{(-\varsigma^2+\tau^2)\mathcal{S}}\right) - \tau\sqrt{\mathcal{S}}\sin\left(2\sqrt{\mathcal{S}}\psi\right)\right)}{\tau\cos\left(2\sqrt{\mathcal{S}}\psi\right)+\varsigma}\right)}. \tag{28}$$

For ($\mathcal{S} > 0$), the KFD framework yields rational fractional wave solution.

$$\mathcal{P}_{15}(x,t) = \frac{m_{-1}\left(c_1 - \frac{c_2}{\psi+\rho}\right)}{\left(-c_2 - \frac{c_1}{\psi+\rho}\right)} + \frac{1}{3}\frac{\beta}{\gamma} + \frac{1}{18}\frac{\beta^2\left(-c_2 - \frac{c_1}{\psi+\rho}\right)}{\gamma^2 m_{-1}\left(c_1 - \frac{c_2}{\psi+\rho}\right)}. \tag{29}$$

4 Planar reformulation of the Reduced fractional equation:

The reduced space-time fractional model, resulting as the Katugampola wave transformation, is a second-order nonlinear ODE whose behaviour captures the qualitative behaviour of the emergent kink excitations. In order to study these properties mathematically tractably, the evolution equation is reformulated in an equivalent planar dynamical-system structure. The re-formulation allows a systematic investigation of the equilibrium landscape and the local stability transitions to transitions to larger phase space structures of the global dynamics of the fractional nonlinear waves. Here, we introduce the trav-

elling wave dynamical variables in order to transform the proposed equation into planar system.

$$z(\psi) = F(\psi), \qquad g(\psi) = \frac{dF}{d\psi}. \tag{30}$$

Thus, equation (12) transforms into the planar dynamical system

$$\begin{cases} \dfrac{dz}{d\psi} = g, \\ \dfrac{dg}{d\psi} = -\dfrac{12}{k\mu^4}\left[(\mu^2 - \omega^2)z + \beta\omega^2 z^2 - \gamma\omega^2 z^3\right]. \end{cases} \tag{31}$$

4.1 Hamiltonian Formulation:

In the present fractional setting, Hamiltonian function takes the form,

$$\begin{cases} \dfrac{dz}{d\psi} = \dfrac{\partial H}{\partial g}, \\ \dfrac{dg}{d\psi} = -\dfrac{\partial H}{\partial z}. \end{cases} \tag{32}$$

$$H(z,g) = \frac{1}{2}g^2 + \frac{6(\omega^2 - \mu^2)}{k\mu^4}z^2 - \frac{4\beta\omega^2}{k\mu^4}z^3 + \frac{3\gamma\omega^2}{k\mu^4}z^4. \tag{33}$$

4.2 Equilibria of the Planar System:

The equilibrium states of the travelling wave dynamics satisfy $\frac{dz}{d\zeta} = 0$ and $\frac{dg}{d\zeta} = 0$, which yield,

$$(z,g) = (0,0), \qquad (z,g) = \left(\frac{\beta\omega^2 \pm \sqrt{\beta^2\omega^4 + 4\gamma\omega^2(\mu^2 - \omega^2)}}{2\gamma\omega^2}, 0\right), \tag{34}$$

provided that, the discriminant is nonnegative:

$$\beta^2\omega^4 + 4\gamma\omega^2(\mu^2 - \omega^2) \geq 0.$$

4.3 Jacobian matrix:

The Jacobian matrix of the system is

$$J(z,g) = \begin{pmatrix} \frac{\partial z'}{\partial z} & \frac{\partial z'}{\partial g} \\ \frac{\partial g'}{\partial z} & \frac{\partial g'}{\partial g} \end{pmatrix} = \begin{pmatrix} 0 & 1 \\ -\frac{12}{k\mu^4}\left[(\mu^2 - \omega^2) + 2\beta\omega^2 z - 3\gamma\omega^2 z^2\right] & 0 \end{pmatrix}.$$

Thus, the jacobian at equilibria are,

$$J(0,0) = \begin{pmatrix} 0 & 1 \\ -\dfrac{12(\mu^2-\omega^2)}{k\mu^4} & 0 \end{pmatrix},$$

$$J(z_*,0) = \begin{pmatrix} 0 & 1 \\ -\dfrac{12}{k\mu^4}\left[(\mu^2-\omega^2)+2\beta\omega^2 z_* - 3\gamma\omega^2 z_*^2\right] & 0 \end{pmatrix},$$

with eigenvalues

$$\lambda_{1,2} = \pm i\sqrt{\frac{12(\mu^2-\omega^2)}{k\mu^4}}.$$

Equilibrium (z,g)	**Characteristic Equation**	**Eigenvalues**	**Nature / Stability**
$(0,0)$	$\lambda^2 + \dfrac{12(\mu^2-\omega^2)}{k\mu^4} = 0$	$\lambda_{1,2} = \pm\sqrt{\dfrac{12(\mu^2-\omega^2)}{k\mu^4}}$	$\mu^2 > \omega^2$: Saddle (Unstable) $\mu^2 < \omega^2$: Center (Stable)
$(z_+,0)$	$\lambda^2 - \dfrac{24\gamma\omega^2 z_+^2 - 12\beta\omega^2 z_+ - 12(\mu^2-\omega^2)}{k\mu^4} = 0$	$\lambda_{1,2} = \pm i\sqrt{\dfrac{24\gamma\omega^2 z_+^2 - 12\beta\omega^2 z_+ - 12(\mu^2-\omega^2)}{k\mu^4}}$	If $\Delta_+ > 0$: Center (Stable) If $\Delta_+ < 0$: Saddle (Unstable)
$(z_-,0)$	$\lambda^2 - \dfrac{24\gamma\omega^2 z_-^2 - 12\beta\omega^2 z_- - 12(\mu^2-\omega^2)}{k\mu^4} = 0$	$\lambda_{1,2} = \pm i\sqrt{\dfrac{24\gamma\omega^2 z_-^2 - 12\beta\omega^2 z_- - 12(\mu^2-\omega^2)}{k\mu^4}}$	If $\Delta_- > 0$: Center (Stable) If $\Delta_- < 0$: Saddle (Unstable)

Table 1: Stability classification of the equilibrium states for the proposed fractional model (1).

4.4 Chaotic Analysis via Time-Periodic Perturbation:

In order to study the onset of nonconservative dynamics and possible switches between regular and chaotic states, we apply a weak external time-periodic perturbation to the planar dynamical system that represents the leading evolution equation of the fractional model:

$$\frac{dF}{d\psi} = G, \qquad \frac{dG}{d\psi} = \frac{6(\omega^2-\mu^2)}{k\mu^4}F - \frac{12\beta\,\omega^2}{k\mu^4}F^2 + \frac{12\gamma\,\omega^2}{k\mu^4}F^3 + r_0\cos(\vartheta\psi), \tag{35}$$

, In which (r_0) and (ϑ) represent the amplitude and frequency of the external forcing, respectively. This time-periodic term introduces dynamical effects into the original system that are not conservative, including resonance overlap, bifurcation cascades, quasi-periodic oscillations and deterministic chaos. The interaction between the cubic nonlinearity and the defraction-order effects increases the sensitivity to the initial condition that produces complex patterns of trajectories in the phase space. In order to measure chaoticity, we use diagnostics of Lyapunov exponent, i.e. the largest Lyapunov exponent λ_{max}. $\lambda_{max} > 0$ indicates chaotic behavior, $\lambda_{max} = 0$ indicates quasi periodical motion and $\lambda_{max} < 0$ indicates asymptotic convergence. At local equilibrium points, local dynamics are regulated by the eigenvalue structure of the Jacobian matrix of the unperturbed system. Centers are associated with neutrally stable oscillatory motion with purely imaginary eigenvalues, and unstable manifolds are associated with saddle points that have real eigenvalues of opposite sign. The disturbances under periodic forcing

can be enhanced by these unstable directions leading to complex responses, including the possibility of chaotic behavior. This perturbation study brings out the subtle interaction between nonlinearity, fractional-order effects, and time-periodic excitation, which shows potential transitions between stable periodic equilibria and chaotic states in the KFD fractional nonlinear system.

5 Results and Discussion:

We analytically explore a space-time fractional Kerr-type nonlinear model. The fractional evolution equation can be solved through a generalized Riccati-Bernoulli sub-ODE scheme and Bäcklund transformation to a first-order nonlinear ODE solvable in closed form, which gives breather-type solutions. These dynamics are studied using 3D surfaces of integer-order dynamics and 2D profiles of the impact of fluctuations in the fractional-order on the amplitude localization, temporal oscillations and stability. All graphical representations are generated using specific parameter values, $c_1 = 0.1$, $c_2 = 0.5$, $\mu = 0.8$, $\beta = 1.2$, $m_{-1} = 0.3$ and $\gamma = 0.5$. More information is gained as per bifurcation diagrams, sensitivity analysis and Lyapunov-based chaos diagnostics, where stable periodic oscillations are observed to turn into quasi-periodic and chaotic conditions. The findings show that the Riccati-Bernoulli Bäcklund framework is a powerful tool in the study of periodic and breather soliton dynamics of fractional nonlinear systems.

The analytical solutions to the dynamical field equations give intriguing kink-type dynamics of the dynamical field profiles under both integer and fractional differentiation. The bright kink structures manifested in the 3D surface plots Figures 1–5, obtained at integer-order parameters show a smooth evolution of the structures along the spatiotemporal plane (x, t). These surfaces are monotonic with time, which means that the solution maintains its localized topological nature in propagation. The kinks are increasing in the negative energy region and approach a flat line as (x) increases, indicating that the system is capable of supporting long-range coherent transport in the nonlinear wave media. This is because such preservation of the kink state during integer-order evolution underscores the stability of the resulting Riccati-Bernoulli type solutions and validates the efficacy of the modelling methodology in describing smooth soliton transportation devoid of oscillatory breakup.

The fractional orders $(\alpha = 1.0, 0.9, 0.8, 0.7)$ plots of 2D are made to clearly display the effects of the nonlocal memory. For $(\alpha < 1)$, the profile of a kink becomes even deeper and sharper as it approaches the transition center, forming a more abrupt gradient and a stronger localization. This is true to the fact that, fractional differentiation discourages dispersion and tightening of the waves, thus making the valley region stronger and the tail narrow. The lowest and most localized depression is found at $(\alpha = 0.70)$ with the highest fractional response. The integer-order $(\alpha = 1.0)$ curve, by contrast, is less jagged and more diffuse, indicating a more powerful dispersion. The trends ensure that the use of fractional order is a tuning parameter, which enables modulation of kink depth, width, and the stability of propagation to control.

Figure 4 shows a significant difference in that profile switches to a dark kink structure instead of a bright kink. This non-linearity parameter-induced inversion implies a phase change in the nonlinear medium by predicting the sensitive interaction of fractional order, dispersion intensity, and nonlinear self-interaction. Such dark kinks are technologically significant since they correspond to intensity dips

on a uniform continuous background, which allow optical switching, inverse-polarity wave transport, and defect-type excitations which can be controlled.

The appearance of bright and dark kink structures in the fractional electrical model is of immediate interest to a number of contemporary physical and engineering problems where non-locality and memory effects dominate the propagation of waves. Bright kinks, displayed in the majority of the figures, are similar to stable energy carrying fronts, and are used extensively in signal transport in fractional transmission lines, on meta-surfaces and in nano-circuits, where low-loss switching and pulse sharpening are critically required. Conversely, the dark kink (Figure 4) is an energy depletion into a homogeneous background, which is typical of optical wave guides, negative-index meta materials, photo refractive materials and Bose-Einstein condensates with repulsive inter-particle interactions. The sensitivity of solution profiles to fractional order (α) suggests the ability to control dispersion by controllable fractional low-pass circuit schemes, pulse shaping at ultra fast speeds in photonics, frequency selective filters, and control of stability in neuronal or biological networks of impulse propagation. Since a localization of the waveforms in the presence of fractional dynamics and a reduction in spreading of the same by lower (α) frequencies, the model is likewise in line with current studies of fractional spin chains, viscoelastic signal transportation, and memory-dependent energy routing in neurotrophic computing channels. Therefore, the bright dark kink spectrum generated by the model emphasizes high potential of application in the real-world in fractional wave-guided energy transfer, reconfigurable photonic logic, soliton-based switching, compact signal processing, and biomimetic communication pathways.

Figure 6 represents the distribution of the total energy of fractional electrical model of the (z,g)-plane. Figure 6(a) depicts the multi-well energy profile on the 3D surface where the peaks are high and valleys are deep suggesting that the phase space has got both stable and unstable regions. This topography indicates that the system has the ability to change between energy wells in response to perturbation, which indicates its nonlinear sensitivity. Figure 6(b) gives the corresponding contour map that provides a top-view of the same structure, with the marked closed loops outlining the bounded low-energy regions and the long curves representing transition pathways. Collectively, these plots indicate how slight changes in the state variables can considerably influence the stored system energy which form a visual foundation of the periodic and complex traits.

Figures 7(a-c) all demonstrate the important dynamical characteristics of the fractional nonlinear electrical model. Figure 7(a) phase diagram illustrates an eye-shaped separatrix which forms around the central family of periodic orbits which are closed and which is an indicator of stable oscillatory behaviour. The phase diagram depicts two saddle points situated where the separatrix eye-shaped region intersects the family of closed periodic orbits. This structure is strengthened by the vector field in Figure 7(b) in which the direction of smooth rotation around the center is evident with the typical diverging-converting pattern of the saddles which affirm the topology of the system is of a Hamiltonian kind and that sensitivity to initial conditions occurs in regions. Figure 7(c) time evolution plots show sustained, almost sinusoidal oscillations in (z) and (g) of constant amplitude that show long-term coherent periodic behavior and the anticipated relationship between the state variable and its derivative in phase. The combination of these numbers confirm the existence of periodic stable dynamics, the contribution of separatrices created by saddles, and the non-dissipative nature of the structure of the fractional model.

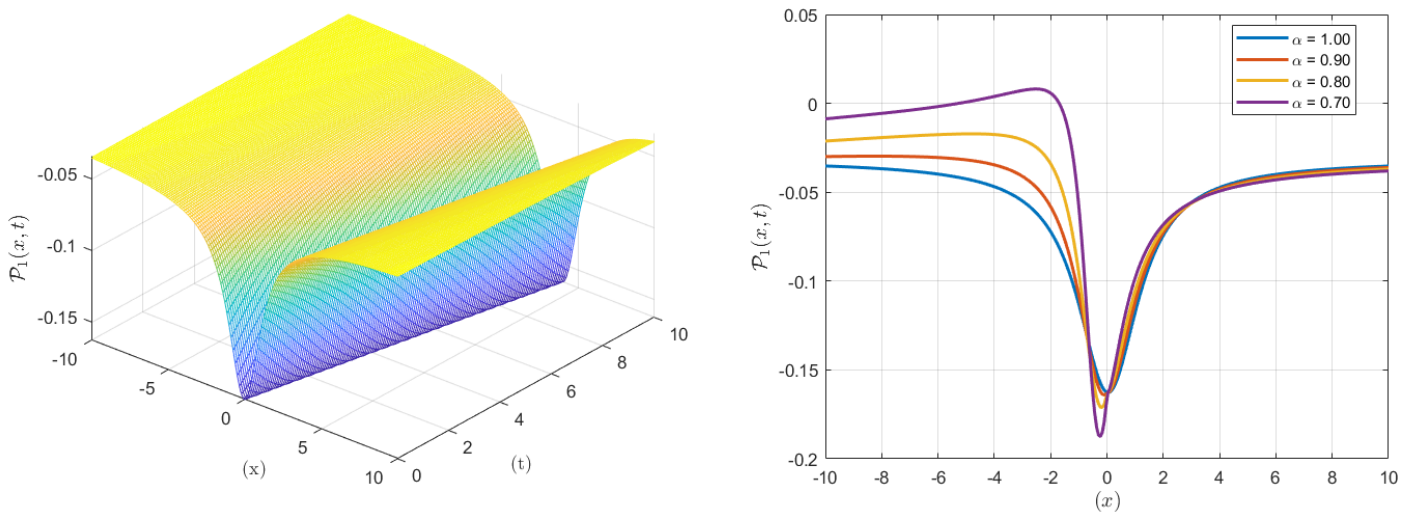

(a) (b)

Figure 1: The solution $\mathcal{P}_1(x,t)$ is visualized using 3D and 2D profiles, highlighting the qualitative differences between integer and fractional order dynamical regimes.

Figures 7(a) and 7(b) demonstrate the chaotic study of fractional nonlinear low-pass electrical model using the maximum Lyapunov exponent λ_{max}. Figure 7(a) shows that, λ_{max} opens with a sharp peak around unity, which is strongly sensitive to perturbations, and quickly decays to a small positive value, signaling the transition between transient chaos and a weakly chaotic steady state consistent with the nonlinear flow seen in both the Hamilton and phase-portrait diagrams. Figure 7(b) also indicates that, λ_{max} reduces monotonically with (β), indicating that there is parameter-based transition between chaotic and quasi-periodic or near-regular dynamics. All of these diagnostics are indicative of the fact that the fractional framework not only alters the dynamical properties of the system in question but also expands the dynamical range within the framework, supporting the flexibility and richness of the Katugampola-based fractional extension.

6 Conclusion:

We have provided an analytical investigation of a space-time fractional nonlinear electrical model based on the Katugampola fractional derivative. A generalized version of Riccati-Bernoulli subODE scheme is used to solve the governing equation with a Bäcklund transformation. This method has the precise solutions as bright and dark kink-type traveling waves. Graphical representations are used to explore the spatiotemporal development of these solutions. The 3D and 2D plots are a clear evidence of the influences on the amplitude localization, sharpness of the waveform, and stability in the case of integer and fractional-order parameters. Specifically, an increase in the fractional order increases the amplitude localization and reduces the dispersion. The resulting dark and bright kink structures have been noted to be of potential use in controlled energy transport, optical switching and nonlinear signal processing in the fractional waveguide systems. Moreover, the phase portraits, Lyapunov-based diagnostics and Hamilton analysis are used to study the dynamical behavior of the model. These studies validate

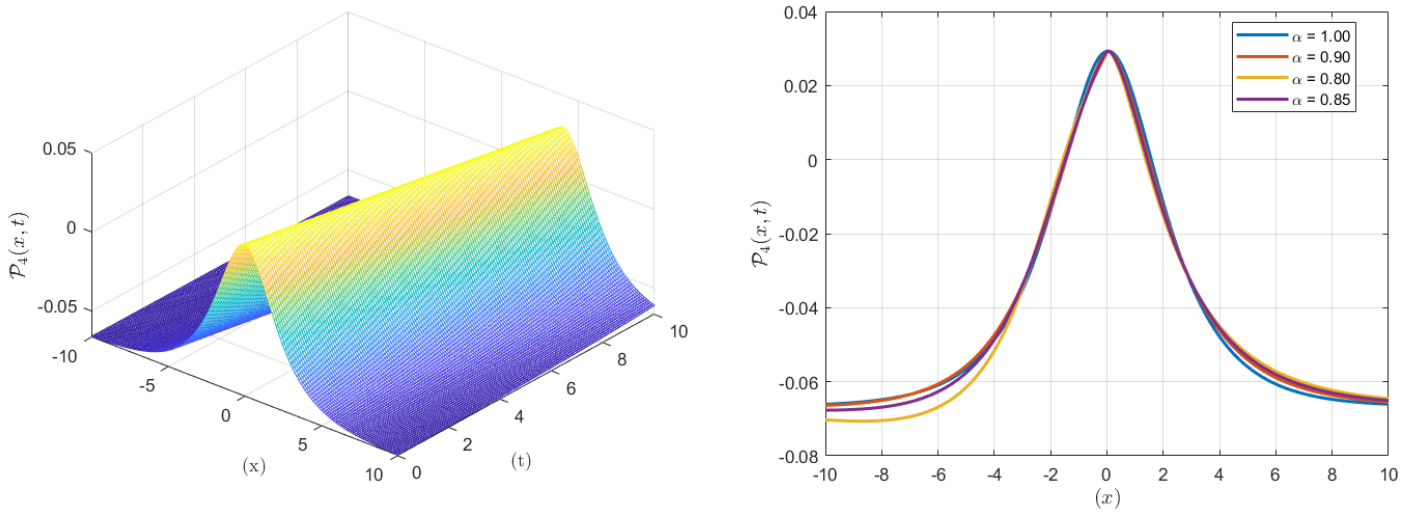

(a) (b)

Figure 2: The solution $\mathcal{P}_4(x,t)$ is visualized using 3D and 2D profiles, highlighting the qualitative differences between integer and fractional order dynamical regimes.

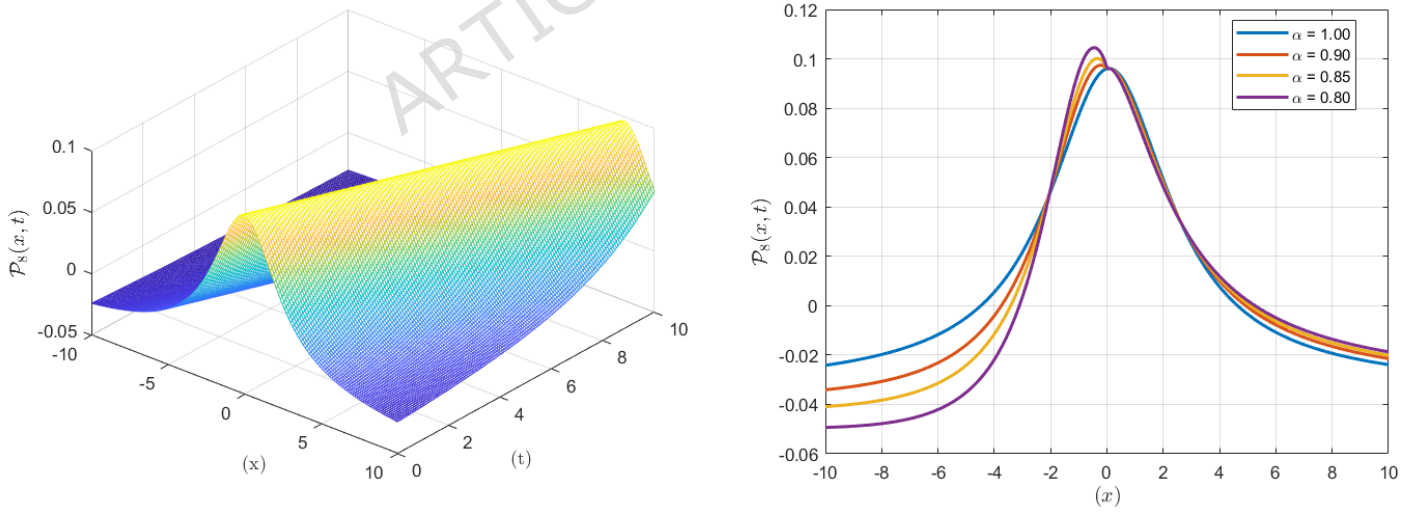

(a) (b)

Figure 3: The solution $\mathcal{P}_8(x,t)$ is visualized using 3D and 2D profiles, highlighting the qualitative differences between integer and fractional order dynamical regimes.

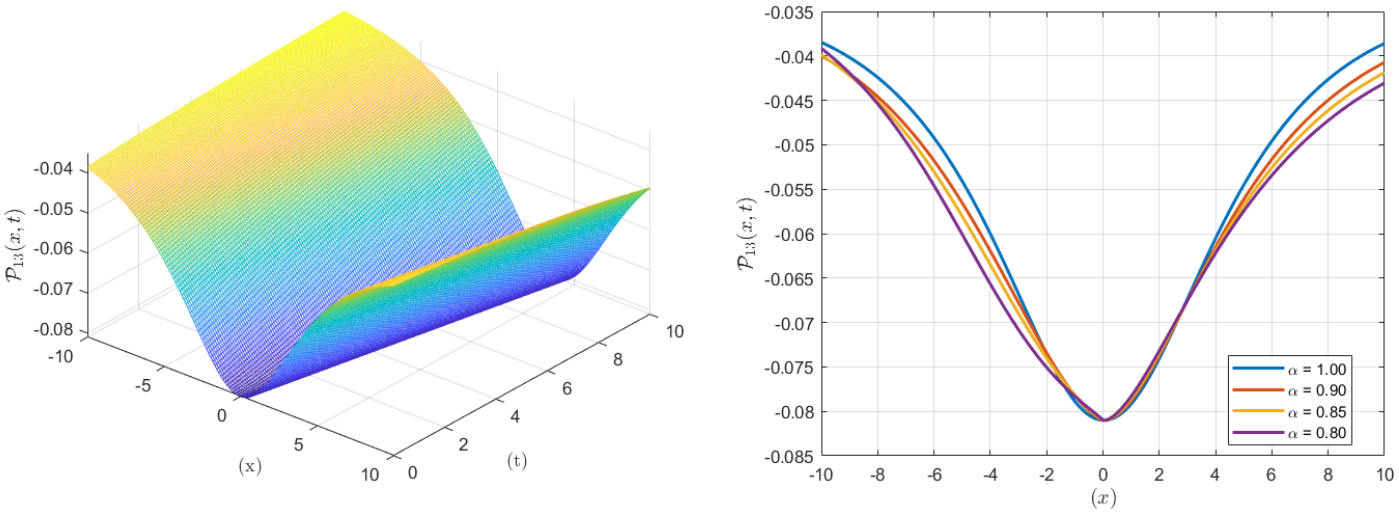

(a) (b)

Figure 4: The solution $\mathcal{P}_{13}(x,t)$ is visualized using 3D and 2D profiles, highlighting the qualitative differences between integer and fractional order dynamical regimes.

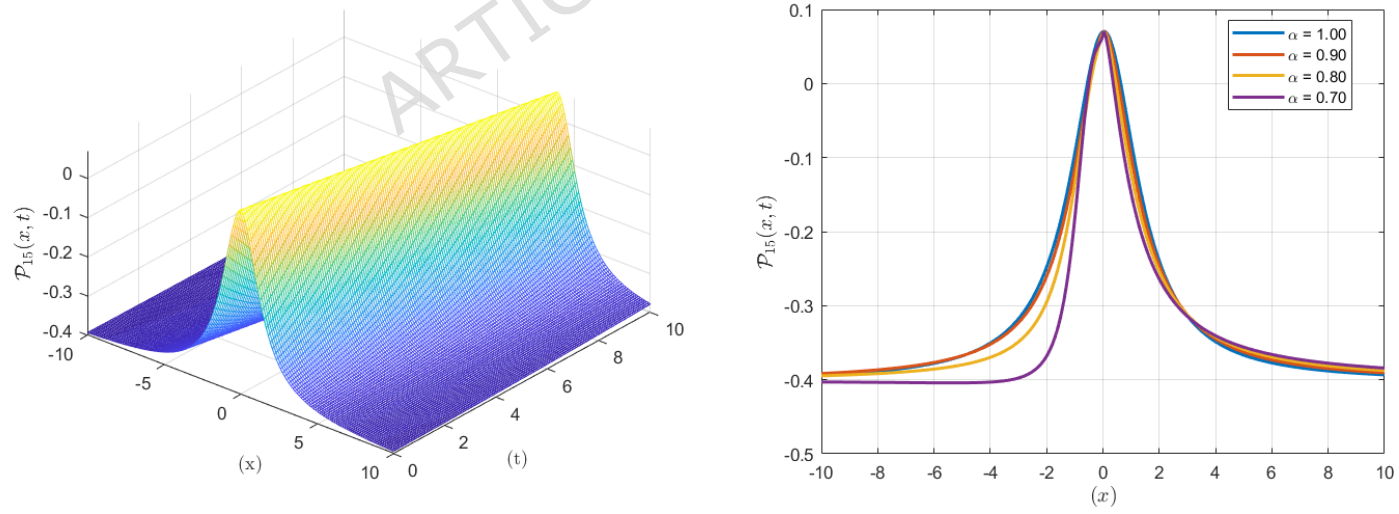

(a) (b)

Figure 5: The solution $\mathcal{P}_{15}(x,t)$ is visualized using 3D and 2D profiles, highlighting the qualitative differences between integer and fractional order dynamical regimes.

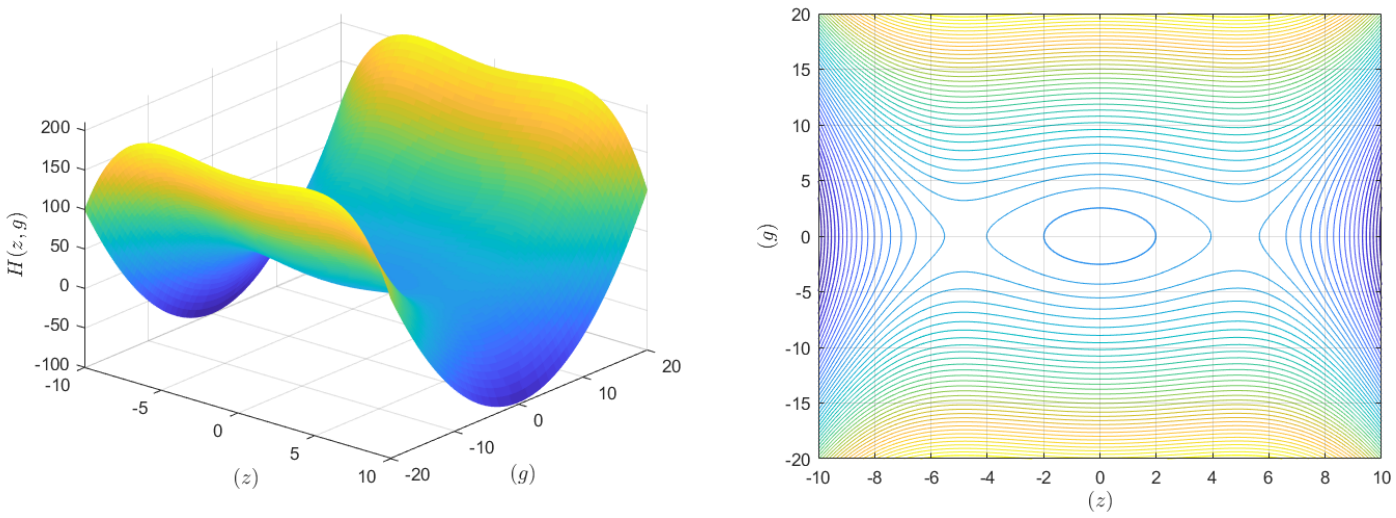

(a) (b)

Figure 6: Energy density distribution derived from equation (33), depicting the evolution of localized energy and its influence on the system's dynamical transitions.

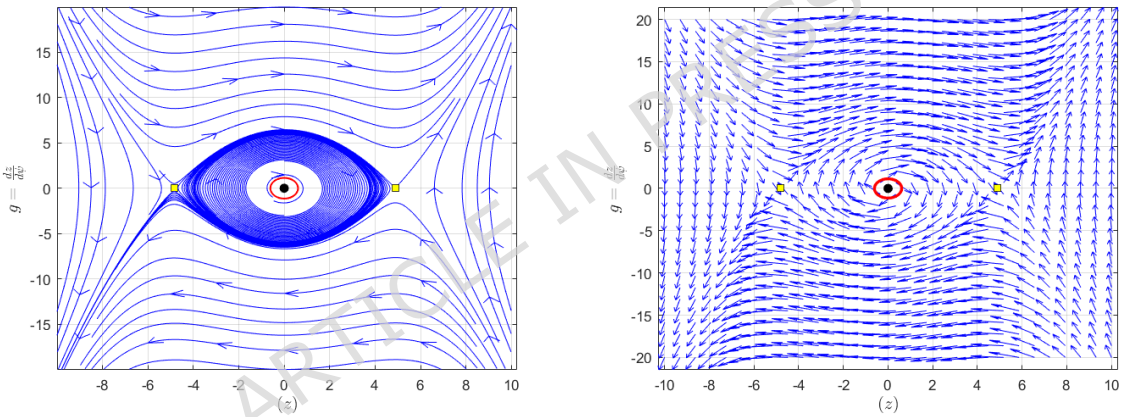

(a) (b)

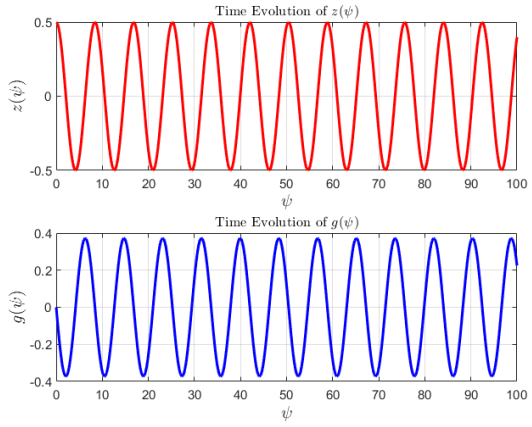

(c)

Figure 7: Phase-portrait and time series plots corresponding to equation (31) and equation (35), revealing the stability behavior of the underlying dynamical system.

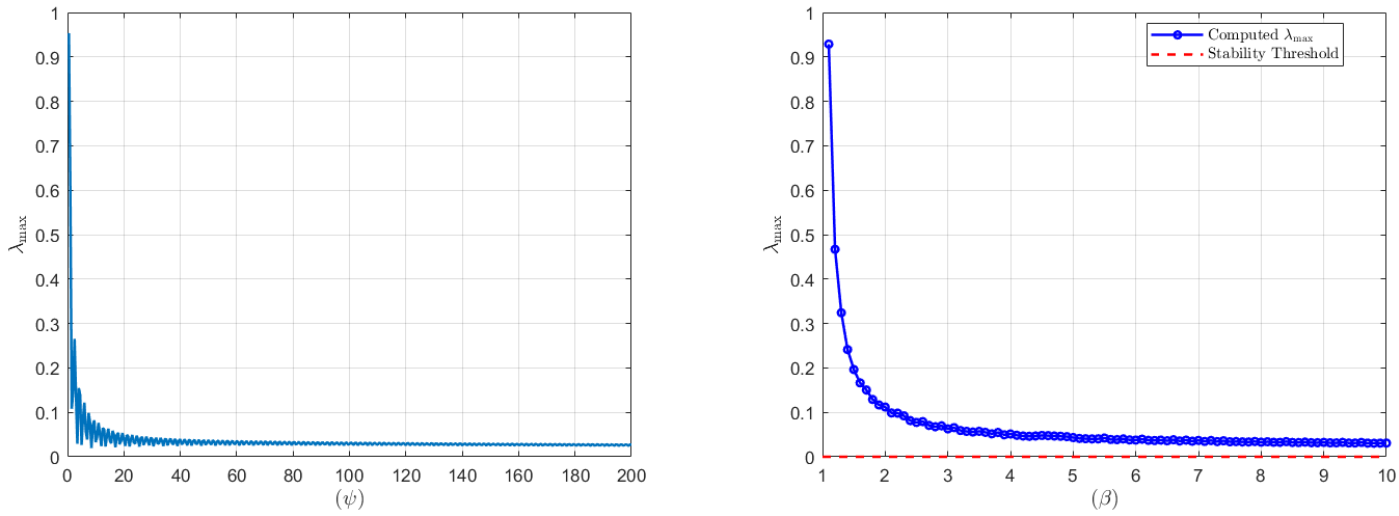

(a) (b)

Figure 8: The first figure validates the asymptotic convergence of the largest lyapunov exponent along (ψ) ensuring numerical stability, the second illustrates the dependence of λ_{max} on (β), indicating a clear transition from regular dynamics to chaos.

the existence of stable periodic, quasi periodic, and chaotic regimes. Multi-well structures are also identified in energy-density distributions, which means that these distributions are highly sensitive to initial conditions and external perturbations. Comprehensively, the findings indicate that the fractional Riccati-Bernoulli-Bäcklund model is a useful model to examine the complex nonlinear waves. It can also offer a versatile and programmable platform to photonics, metamaterials, fractional transmission lines and biomimetic communication applications.

Author contributions

Zainab Alsheekhhussain, Rasool Shah, Hashmatullah Sanaee, Saleh Alshammari, Mohammad Alshammari, M. Mossa Al-sawalha; Conceptualization, methodology, software, validation, formal analysis, investigation, resources, data curation, writing-original draft preparation, writing-review and editing, visualization, supervision, project administration. All authors have read and agreed to the published version of the manuscript.

Acknowledgement

This research has been funded by Scientific Research Deanship at University of Ha'il - Saudi Arabia through project number $< RG - 25 \quad 110 >$

Data Availability

The datasets used and/or analysed during the current study available from the corresponding author on reasonable request.

Funding

Not applicable.

Consent for publication

"Not applicable" in this section.

Ethics declaration

Not applicable.

Competing interests

The authors declare no competing interests.

References

[1] Kalita, J., Das, R., Hosseini, K., Baleanu, D., Salahshour, S. Solitons in magnetized plasma with electron inertia under weakly relativistic effect. *Nonlinear Dynamics*, **111**, 37013711, 2023.

[2] Zhang, H. Q., Wang, D. S. Wave solutions of the Mikhailov-Novikov-Wang equation by the improved F-expansion method. *Applied Mathematics and Computation*, **233**, 429437, 2014.

[3] Dai, J., Zhang, S., Tian, S. Optimization of wave propagation in a graphene system with spatially varying masses. *Journal of Physics: Condensed Matter*, **27**, 055303, 2015.

[4] Naeem, M., Rezazadeh, H., Khammash, A.A., and Zaland, S., 2022. Analysis of the Fuzzy Fractional-Order Solitary Wave Solutions for the KdV Equation in the Sense of Caputo-Fabrizio Derivative. Journal of Mathematics, 2022(1), p.3688916.

[5] Yasmin, H., Alshehry, A.S., Ganie, A.H., Shafee, A. 2024. Noise effect on soliton phenomena in fractional stochastic Kraenkel-Manna-Merle system arising in ferromagnetic materials. Scientific Reports, 14(1), p.1810.

[6] Alqhtani, M., Saad, K.M., Weera, W. and Hamanah, W.M., 2022. Analysis of the fractional-order local Poisson equation in fractal porous media. Symmetry, 14(7), p.1323.

[7] Shah, R., Alkhezi, Y. and Alhamad, K., 2023. An analytical approach to solve the fractional Benney equation using the q-homotopy analysis transform method. Symmetry, 15(3), p.669.

[8] Shafee, A., Alkhezi, Y. 2023. Efficient solution of fractional system partial differential equations using Laplace residual power series method. Fractal and Fractional, 7(6), p.429.

[9] Kumar, S., Rani, S. Invariance analysis, optimal system, closed-form solutions and dynamical wave structures of a (2+1)-dimensional dissipative long wave system. *Physica Scripta*, **96**, 125202, 2021.

[10] Guan, X., Liu, W., Zhou, Q., Biswas, A. Darboux transformation and analytic solutions for a generalized super-NLS-mKdV equation. *Nonlinear Dynamics*, **98**, 14911500, 2019.

[11] Feng, Y., Bilige, S. Multiple rogue wave solutions of (2+1)-dimensional YTSF equation via Hirota bilinear method. *Waves in Random and Complex Media*, **34**, 94110, 2024.

[12] Kumar, S., Mohan, B. A study of multi-soliton solutions, breather, lumps, and their interactions for Kadomtsev-Petviashvili equation with variable time coefficient using Hirota method. *Physica Scripta*, **96**, 125255, 2021.

[13] Kumar, S., Niwas, M., Hamid, I. Lie symmetry analysis for obtaining exact soliton solutions of generalized CamassaHolmKadomtsevPetviashvili equation. *International Journal of Modern Physics B*, **35**, 2150028, 2021.

[14] Yang, J. Y., Ma, W. X., Qin, Z. Lump and lump-soliton solutions to the (2+1)-dimensional Ito equation. *Analysis and Mathematical Physics*, **8**, 427436, 2018.

[15] Kaup, D. J. The lump solutions and the Bäcklund transformation for the three-dimensional three-wave resonant interaction. *Journal of Mathematical Physics*, **22**, 11761181, 1981.

[16] Zhang, H. Q., Ma, W. X. Lump solutions to the (2+1)-dimensional SawadaKotera equation. *Nonlinear Dynamics*, **87**, 23052310, 2017.

[17] Chen, S. T., Ma, W. X. Lump solutions to a generalized Bogoyavlensky-Konopelchenko equation. *Frontiers of Mathematics in China*, **13**, 525534, 2018.

[18] Rodwell, M. J. W., Kamegawa, M., Yu, R., Case, M., Carman, E., Giboney, K. GaAs nonlinear transmission lines for picosecond pulse generation and millimeter-wave sampling. *IEEE Transactions on Microwave Theory and Techniques*, **39**, 11941204, 1991.

[19] Seadawy, A. R., Iqbal, M., Baleanu, D. Construction of traveling and solitary wave solutions for wave propagation in nonlinear low-pass electrical transmission lines. *Journal of King Saud University – Science*, **32**, 2752–2761, 2020.

[20] Abdoulkary, S., Beda, T., Dafounamssou, O., Tafo, E. W., Mohamadou, A. Dynamics of solitary pulses in the nonlinear low-pass electrical transmission lines through the auxiliary equation method. *Journal of Modern Physics and Applications*, **2**, 6987, 2013.

[21] Kayum, M. A., Akbar, M. A., Osman, M. S. Competent closed form soliton solutions to the nonlinear transmission and the low-pass electrical transmission lines. *European Physical Journal*, **135**, 120, 2020.

[22] Kumar, H., Kumar, A., Chand, F., et al. Construction of new traveling and solitary wave solutions of a nonlinear PDE characterizing the nonlinear low-pass electrical transmission lines. *Physica Scripta*, **96**, 085215, 2021.

[23] Kumar, D., Seadawy, A. R., Haque, M. R. Multiple soliton solutions of the nonlinear partial differential equations describing the wave propagation in nonlinear low-pass electrical transmission lines. *Chaos, Solitons & Fractals*, **115**, 62–76, 2018.

[24] Banchuin, R. On the noise performances of fractal-fractional electrical circuits. *International Journal of Circuit Theory and Applications*, **51**, 8096, 2023.

[25] Sikora, R., Pawiowski, S. Fractional derivatives and the laws of electrical engineering. *COMPEL The International Journal for Computation and Mathematics in Electrical and Electronic Engineering*, **37**, 13841391, 2018.

[26] Wang, K. L. Novel perspective to the fractional Schrdinger equation arising in optical fibers. *Fractals*, **32**, 2450034, 2024.

[27] Park, C., Khater, M. M. A., Attia, R. A. M., et al. An explicit plethora of solutions for the fractional nonlinear model of the low-pass electrical transmission lines via Atangana-Baleanu derivative operator. *Alexandria Engineering Journal*, **59**, 12051214, 2020.

[28] Almusawa, H., Jhangeer, A., Munawar, M. Analytical analyses for a fractional low-pass electrical transmission line model with dynamic transition. *Symmetry*, **14**, 1377, 2022.

[29] Zulfiqar, A., Ahmad, J., Rani, A., et al. Wave propagations in nonlinear low-pass electrical transmission lines through optical fiber medium. *Mathematical Problems in Engineering*, **2022**, 116, 2022.

[30] Li, Z. Solving the exactly explicit solutions of the conformable space-time fractional Phi-4 equation via neural networks method. *Physics Letters A*, **2026**, 131535, 2026.

[31] Tang, C., Li, X., Wang, Q. Solvability of indefinite stochastic LQ optimal control problems for jump diffusion models. *Journal of Dynamical and Control Systems*, **32**(1), 911, 2026.

[32] Wang, J., Li, Z. The impact of standard Wiener process on the qualitative analysis and traveling wave solutions of stochastic nonlinear Kodama equation in the Stratonovich sense. *AIMS Mathematics*, **10**(10), 2499725010, 2025.

[33] Noor, S., Alshehry, A.S., Shafee, A. 2024. Families of propagating soliton solutions for (3+ 1)-fractional Wazwaz-BenjaminBona-Mahony equation through a novel modification of modified extended direct algebraic method. Physica Scripta, 99(4), p.045230.

[34] Naeem, M., Azhar, O.F., Zidan, A.M., Nonlaopon, K. and Shah, R., 2021. Numerical Analysis of Fractional-Order Parabolic Equations via Elzaki Transform. Journal of Function Spaces, 2021(1), p.3484482.

[35] Shah, R., Saad Alshehry, A. and Weera, W., 2022. A semi-analytical method to investigate fractional-order gas dynamics equations by Shehu transform. Symmetry, 14(7), p.1458.

[36] Sunthrayuth, P., Shah, R., Zidan, A.M., Khan, S. and Kafle, J., 2021. The Analysis of Fractional-Order Navier-Stokes Model Arising in the Unsteady Flow of a Viscous Fluid via Shehu Transform. Journal of Function Spaces, 2021(1), p.1029196.

[37] Al-Sawalha, M.M., Yasmin, H., Shah, R., Ganie, A.H. and Moaddy, K., 2023. Unraveling the dynamics of singular stochastic solitons in stochastic fractional KuramotoSivashinsky equation. Fractal and Fractional, 7(10), p.753.

[38] Phoosree, S., Khongnual, N., Sanjun, J., Kammanee, A., Thadee, W. Riccati sub-equation method for solving fractional flood wave equation and fractional plasma physics equation. *Partial Differential Equations in Applied Mathematics*, **10**, 100672, 2024.

[39] Yang, X.F., Deng, Z.C., Wei, Y. A Riccati-Bernoulli sub-ODE method for nonlinear partial differential equations and its application. *Advances in Difference Equations*, **2015**(1), 117–133, 2015.

[40] Abdelrahman, M.A.E., Sohaly, M.A. Solitary waves for the nonlinear Schrödinger problem with the probability distribution function in the stochastic input case. *European Physical Journal Plus*, **132**, 339, 2017.

[41] Katugampola, U.N. A new fractional derivative with classical properties. *arXiv preprint*, arXiv:1410.6535, 2014.